Continuous real-time bubble monitoring in microchannels using refractive index detection

INSTITUTE OF PHYSICS PUBLISHING MEASUREMENT SCIENCE AND TECHNOLOGY
Meas. Sci. Technol. **15** (2004) 290–296 PII: S0957-0233(04)67993-8

Continuous real-time bubble monitoring in microchannels using refractive index detection

Shee-Ann Leung, Joshua B Edel, Robert C R Wootton and Andrew J deMello

Department of Chemistry, Imperial College London, South Kensington, London SW7 2AZ, UK

E-mail: a.demello@ic.ac.uk

Received 20 August 2003, in final form 29 October 2003, accepted for publication 12 November 2003
Published 28 November 2003
Online at stacks.iop.org/MST/15/290 (DOI: 10.1088/0957-0233/15/1/042)

Abstract
A novel approach to the monitoring and analysis of bubbles in gas/liquid binary systems is described. The method is based on the varying extent of refraction experienced by radiation as it passes through a gas or liquid. Specifically, carbonated liquids are hydrodynamically motivated through a microfluidic channel network (40 μm wide and 30 μm deep) and directed through the path of laser beam. As a gas bubble passes through this region, the reduction in local refractive index leads to an increased displacement of the laser beam which is monitored using a position-sensitive detector. Statistical analysis of multiple bubble events (in terms of autocorrelation curves, burst width distributions and interburst time curves) yields information relating to both the bubble size and the frequency of bubble formation.

Keywords: microchannel, refractive index detection, bubble analysis, microfluidics

(Some figures in this article are in colour only in the electronic version)

1. Introduction

The analysis of small gas bubbles in biological and industrial systems has received much attention. For example, many organic reactions include reactants or generate products in the gas phase. Such reactions include the hydrogenation of alkenes and diazonium chemistries, particularly Sandmeyer reactions [1]. In such reactive systems, information relating to reaction kinetics such as rate of reaction and reaction yield can be obtained *in situ* simply by the quantification of gas bubbles during a reaction. In the oil exploration industry, gas bubbles in bore-holes are an indication of potential explosion hazards [2]. Bubbles are formed in slurries when the drill is about to enter a high-pressure gas pocket. Early detection of these bubbles is recognized as a useful marker to alert operators and prevent catastrophic gas release.

Several attempts at the quantification and analysis of bubble behaviour have been presented. For example, Lin and co-workers [2] utilized a pulse displacement technique to measure the velocity, size and refractive index (RI) of bubbles. Specifically, falling water droplets in oil were used to mimic the behaviour of gas bubbles in a slurry. Bubble detection was effected through illumination of the detection volume with three parallel planes of laser light, and two photodetectors placed above and below the laser planes. As a particle moves through this volume the detectors measure a number of refracted and reflected beams. The temporal relationship between these signals can then be used to calculate particle velocity, size and refractive index.

Barigou and Greaves [3] have also described a capillary suction probe for measurement of bubble size in a stirred-vessel reactor. In this system, gas–liquid dispersions are drawn through a capillary by suction and photodetectors mounted on a tube are used to detect the bubble slugs. Due to variations in refractive index, higher light intensities are registered by a detector when a light beam passes through a liquid slug rather

than a gas slug. The system benefits from simplicity but is limited to the analysis of bubbles greater than 1 mm in diameter. Kawaguchi *et al* [4] have described an interferometric laser imaging technique for droplet and bubble sizing. Using this method, the diameter of spherical transparent particles was determined by measurement of the fringe spacings of the interference pattern. Although this approach is unsuitable for continuous monitoring applications (since size information is recovered through post-measurement image analysis) bubble diameters as low as 200 μm could be measured.

In most gas/liquid systems a wide range of bubble sizes is typical. This means that extraction of mean bubble sizes is most easily and effectively achieved via high-throughput measurement techniques, where statistical analysis of a large population dataset can be used to provide information about average size. The primary problem in performing a large number of measurements in such systems is the ability to detect bubbles quickly and reliably. In broad terms this can only be achieved by either directing bubbles through a defined detection volume (yielding high particle detection efficiencies) or by having a large excess of bubbles in which a smaller fraction are detected. An interesting solution to this problem is to use microfluidic channels to confine and manipulate bubbles within flowing environments.

Over the past decade microfluidic chip systems have been used to great effect in many areas of the physical and biological sciences [5]. These miniaturized analytical instruments employ micromachined features (such as channels, electrodes, reactors and filters) and are able to manipulate fluid samples with high precision and efficiency. Microfluidic chip devices have been used in a wide variety of applications including nucleic acid separations, protein analysis, process control, small-molecule organic synthesis, DNA amplification, immunoassays, DNA sequencing, and cell manipulations [6, 7]. In a fundamental sense, microfluidic systems have been shown to have many advantages over their conventional (larger) analogues. These include improved efficiency with regard to sample size, response times, cost, analytical performance, process control, integration, throughput and automation.

In the current studies microchannels are used as conduits in which bubbles may be motivated along and directed to a defined detection volume. In this way we ensure that bubbles can be detected both efficiently and rapidly. Using conventional lithographic and wet-etching methods, well defined channels (with cross-sectional dimensions in the range of tens to hundreds of microns) can be formed easily in planar glass substrates. Furthermore, the small instantaneous volumes (normally a few nanolitres) associated with these fluidic networks means that consumption of reagents is minimal. An additional advantage of using microfluidic systems to perform bubble analysis is that, due to the closed channels and well-defined dimensions of the system, data such as the viscosity of the fluids studied and the molar quantities of gas in a typical bubble can in principle be adduced. For example, the pressure differential at a given point along a rectangular channel can be defined in terms of fluid viscosity, fluid flow rate and channel dimensions according to equation (1), i.e.

$$\Delta p = \frac{12 v \eta l}{w d^3} \tag{1}$$

where Δp is the pressure differential (N m^{-2}), v is the fluid velocity (m s^{-1}), η is the fluid viscosity (N s m^{-2}), l is the channel length (m), w is the channel width (m) and d is the channel depth (m). In theory the volume (at a known pressure) of any bubble of gas is proportional to the number of moles of gas present. Thus a measure of average gas volume should allow calculation of the average molar size of bubbles.

Herein, a simple and cost-effective detection system for monitoring bubbles within microfluidic channels is described. For demonstration purposes five different carbonated drinks are used as test media. When a carbonated drink is opened the abrupt change in pressure of the can environment from the pressurized container to atmospheric pressure results in formation of gas bubbles. This is due to the perturbation of the prevailing thermodynamic equilibrium within the container [8]. Different sizes and distributions of gas bubbles are created according to a complex set of criteria. Gas bubbles are monitored by a refractive index variation detection system, in which light passing through a microchannel is refracted by the channel contents. The degree of refraction is dependent on the refractive index of the material and can be measured using a position-sensitive detector (PSD).

2. Experimental details

2.1. Materials

Readily available carbonated beverages (The Coca-Cola Company) were studied. They were A (Fanta), B (Coke), C (Sprite) and D (Diet-Coke). Champagne (Monopole Blue Top, Piper-Heidsieck & Co, Epernay) was also analysed. Each sample was opened and immediately transferred into a reservoir. A vacuum pump (KNF, Neuberger Laboport) was then used to motivate the sample via 100 μm inner diameter capillary tubing (Composite Metals, Worcester, UK) into the microfluidic channel at a constant flow rate of 10 μl min^{-1}.

3. Microfabrication

Microfluidic devices were manufactured in-house and comprised a thermally bonded structured glass substrate containing the microchannel network. Microfluidic channel patterns were transferred onto a glass wafer precoated with positive photoresist and chromium (Nanofilm, Westlake Village, CA, USA) using a direct-write photolithographic system (DWL2.0, Heidelberg Instruments, Heidelberg, Germany). Typical channel widths ranged from 5 to 50 μm. The exposed photoresist was then removed using a 5:1 ratio of developing agent (Microposit, Coventry, UK) to water. This was followed by a chromium etching procedure using a Lodyne etch (Microchem Systems, Coventry, UK). The etched substrates were finally rinsed in 18 MΩ water and H_2SO_4–H_2O_2 (50:50). Prior to bonding, 400 μm reservoir access holes were drilled in the coverplate. Bonding between the coverplate and the substrate was performed by heating in a high-temperature oven to a maximum of 610 °C. The top plate was then optically polished down to a thickness of $\sim$150 μm. Finally, 375 μm outer diameter, 100 μm inner diameter Polymicro tubing (Composite Metals, Worcester, UK) was glued to the access holes using Araldite 2014

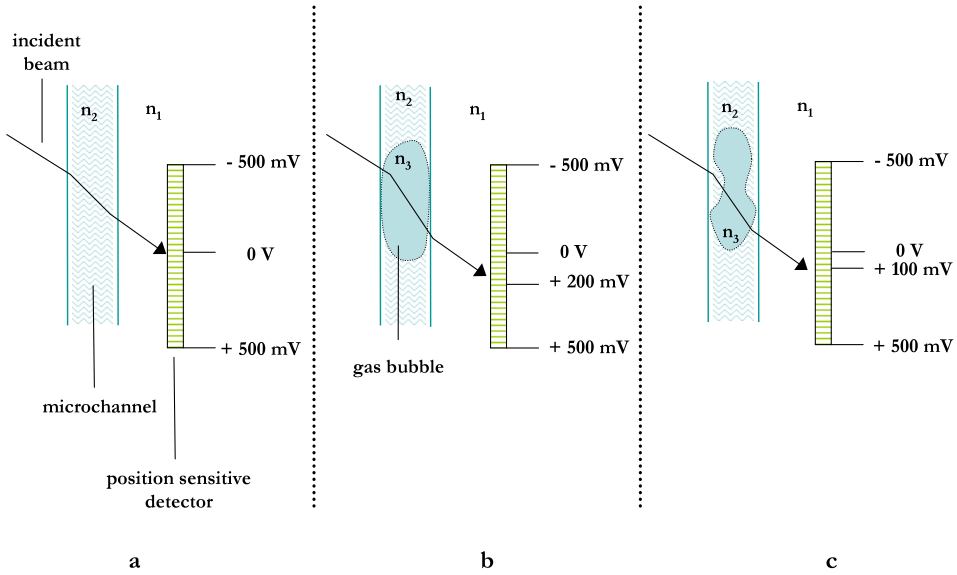

Figure 1. Schematic of the RI detection system under the following conditions: (a) liquid present in the detection volume, (b) a gas bubble completely filling the microchannel and detection volume and (c) a gas bubble that is partially filling the microchannel and detection volume.

(RS Components, UK). A diaphragm vacuum pump (KNF Neuberger Laboport) was used to deliver solutions at a constant flow rate of 10 μl min^{-1} into the capillary tubing.

4. Refractive index detection system

A polarized laser beam (488 nm line from a CW air-cooled argon ion laser, Omnichrome; Melles Griot, Cambridge, UK) was passed through a 50 μm precision pinhole (Melles Griot, Cambridge, UK) and refocused by a 50 mm focal length focusing lens (1 inch, Elliot Scientific Ltd) onto the glass chip through a prism at an angle of 40°.

As laser light passes through the microfluidic channel it is refracted to varying degrees depending on the material within the detection volume (i.e. gas or liquid). The relationship between RI and the extent of refraction is defined according to Snell's law:

$$n_1 \sin\theta_1 = n_2 \sin\theta_2. \qquad (2)$$

Here n_1 is the RI of medium 1 and θ_1 is the angle of incident radiation (to the normal) while θ_2 is the angle of refraction in medium 2 (n_2). Figure 1 shows a schematic of the detection method.

The system is configured so that when liquid is present in the detection volume the PSD registers a voltage reading of 0 V (figure 1(a)). If liquid is replaced by a gas bubble (that completely fills the channel width) a reduction in n_2 occurs and the angle of refraction is shifted away from the normal. For the current experiments the PSD is positioned so that when this occurs a voltage reading of 200 mV is registered (figure 1(b)). In this ideal situation, the presence of the bubble is evidenced by an increase in the detector output from 0 V to 200 mV. However, in many cases a bubble will fail to fill the entire channel width (e.g. figure 1(c)). This results in a smaller variation in the angle of refraction and thus a smaller signal registered at the detector. Consequently, some bubble peaks will be evidenced by peaks of reduced intensity.

As stated, the refracted light is collected by a two-dimensional PSD (S1881, Hamamatsu Photonics UK Ltd). The two-dimensional PSD (with an active area of 22 mm × 22 mm) was mounted onto a signal processing circuit (C4674, Hamamatsu Photonics UK Ltd). The signal processing circuit is designed to provide two-dimensional position data independent of the light intensity. The output signals from the circuit equate to position data of the refracted light in terms of V mm^{-1}. The x and y directional signal outputs are then recorded by a dual-channel analogue–digital converter (ADC100, Pico Technology Ltd). For the current experiments data acquisition was performed at a 10 ms sampling rate.

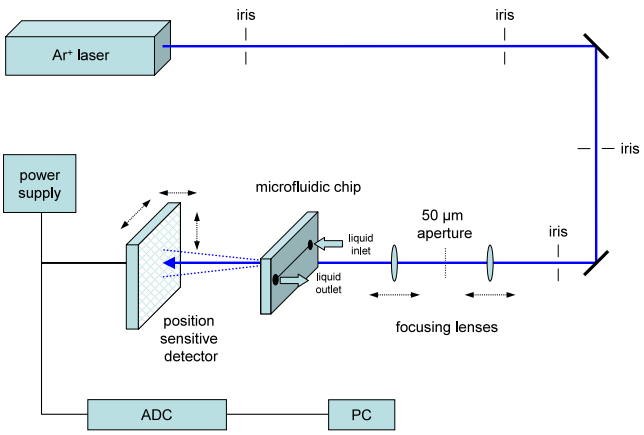

Figure 2. Schematic representation of the experimental set-up. The argon ion laser is aligned and the beam diameter reduced to 50 μm. The laser light is refracted at air/glass and sample/glass interfaces, passes through the microfluidic chip and is detected by the position-sensitive detector.

A schematic representation of the complete experimental set-up is shown in figure 2. Briefly, liquid is motivated into the microfluidic channel by suction through a 100 μm internal diameter capillary. The liquid is sampled from the reservoir (can or bottle) directly into the capillary with no further elaboration.

5. Data analysis

A program written in Matlab 6.5 (Mathworks, Cambridge, UK) was used to determine peak heights, areas, widths and locations as well as for autocorrelation analysis [9]. Briefly, the program searches for a given peak maximum above a specific threshold value which can be defined as three standard deviations from the mean background signal, i.e. $n_{\text{threshold}} = \mu + 3(\mu)^{0.5}$. Adoption of a threshold that lies three standard deviations above the mean yields confidence limits greater than 99%. Once a peak is located, the peak area was determined by analysing a specified number of bins either side of the peak maximum until the background threshold value is reached. The program then searches for the next peak and continuously repeats until all peaks are accounted for. The mean and standard deviation are then calculated for burst heights, areas and widths. Distribution plots are histograms generated from all sampled bursts of a given beverage at a flow velocity of 10 μl min^{-1}.

Autocorrelation analysis was used to quantify respective burst widths in a given sample. This form of analysis essentially measures the average of a fluctuating signal as opposed to the mean spectral intensity. The autocorrelation function, $G(\tau)$, is defined in equation (3):

$$G(\tau) = \sum_{t=0}^{N-1} g(t)g(t+\tau). \tag{3}$$

Here $g(t)$ is the total signal during the time interval $(t, t+\Delta t)$, $g(t+\tau)$ is the signal detected in an interval of Δt at a later time $t+\tau$, and N is the total number of time intervals in the dataset.

6. Results and discussion

A constant flow rate of 10 μl min^{-1} was employed to drive the carbonated beverages through the microfluidic channel. An image of two gas bubbles within the microfluidic channel is shown in figure 3. As previously described, when a gas bubble passes through the detection region in the microfluidic channel, a burst is registered due to a change in RI (from liquid to gas). The duration of residence of the bubble in the detection volume can be measured through analysis of the burst width while the relative change in RI is represented by the burst height.

Some debate was engendered over whether the bubbles observed were nucleated in the reservoir or the sampling capillary. It was noted that bubbles formed in the reservoir rapidly reached a diameter well in excess of 1 mm, which would lead to an extremely wide burst on the detector. Few such bursts were observed. This suggests that the capillary inlet excludes externally formed bubbles to a large degree, and that the bubbles observed were a result of internal nucleation. Thus it appears that the system as configured functions as a method of determining supersaturated gas load within a liquid rather than a method for counting pre-existing bubbles.

In an ideal situation, the change in RI between background liquid (RI $\approx$1.3741) and a carbon dioxide (RI = 1.000 45) bubble acts as an 'on–off' switch on the PSD, creating a burst 200 mV high. However, as noted, carbon dioxide bubbles do not always fill the whole channel when passing through the detection volume, and therefore the burst height represents the relative change in RI in the detection volume. Burst scans of 6 min sections at 5, 20, 35 and 50 min after opening sample A are shown in figure 4. Here each burst represents a single bubble passing through the detection volume. It can be seen that the number of peaks detected per unit time gradually decreases with increasing time. For example, 350 particle bursts are accumulated within the first 6 min (figure 4(a)), whereas between 50 and 56 min (figure 4(d)) only 24 particle bursts are observed. Given the nature of the sample this can be easily understood: the gas/liquid system in the reservoir is equilibrating. Initial outgassing is extremely rapid, but slows over time as the amount of dissolved CO_2 decreases.

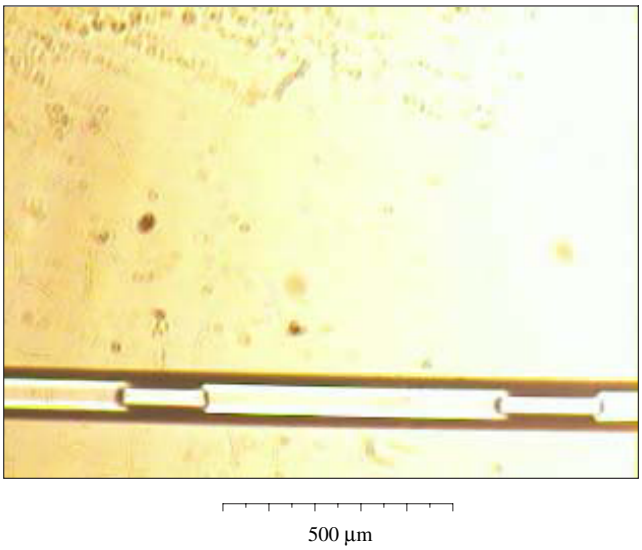

Figure 3. A photograph of two gas bubbles moving through a microfluidic channel (dimensions: 40 μm wide $\times$30 μm deep) at a volumetric flow rate of 10 μl min^{-1}.

The variation in burst height can be explained in terms of the variable degree of filling of the channel by a gas bubble. Bubble flow in a channel can be described in terms of two major regimes, 'bubbly' flow, where the average size of bubble is of the order of the channel width, and 'slug' flow, where the average size of bubble is greater than the channel width. The two regimes function concurrently rather than in well defined states. Slug flow is characterized by bubbles filling the channel, bubbly flow by bubbles travelling through a sheath of fluid within the channel [10]. These systems can be qualitatively examined through analysis of peak heights. The maximum peak height represents the boundary of the slug flow regime. From the data illustrated in figure 1 it can be seen that the flow regime is operating in bubbly flow, with the average peak height decreasing over time. This suggests that the relative size of the generated bubbles also decreases over time.

In the current system, the signal to noise ratio is dependent on the differences in RI between gas and liquid, the dimensions of the microfluidic channel and the size of the gas bubbles with respect to the channel dimension. Good signal to noise ratios were obtained throughout the experiments, indicating that average bubble size was significant with respect to channel dimensions. Burst width distributions for sample A at varying times after opening are shown in figure 5. The average peak width for times of 5 min, 12 and 24 h after opening are

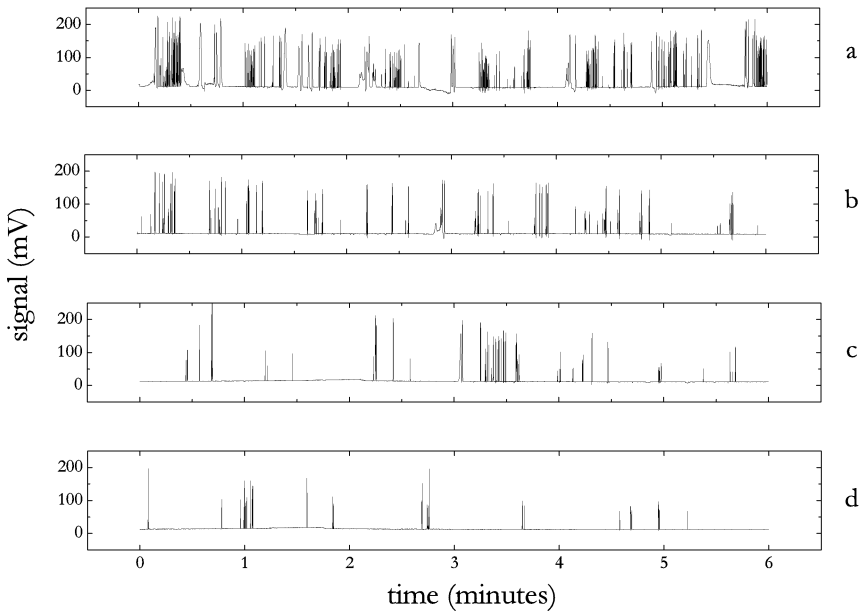

Figure 4. Bubble burst scans (6 min duration) recovered from sample A at: (a) 5 min, (b) 30 min, (c) 35 min and (d) 50 min after opening. Volumetric flow rate = 10 μl min^{-1}.

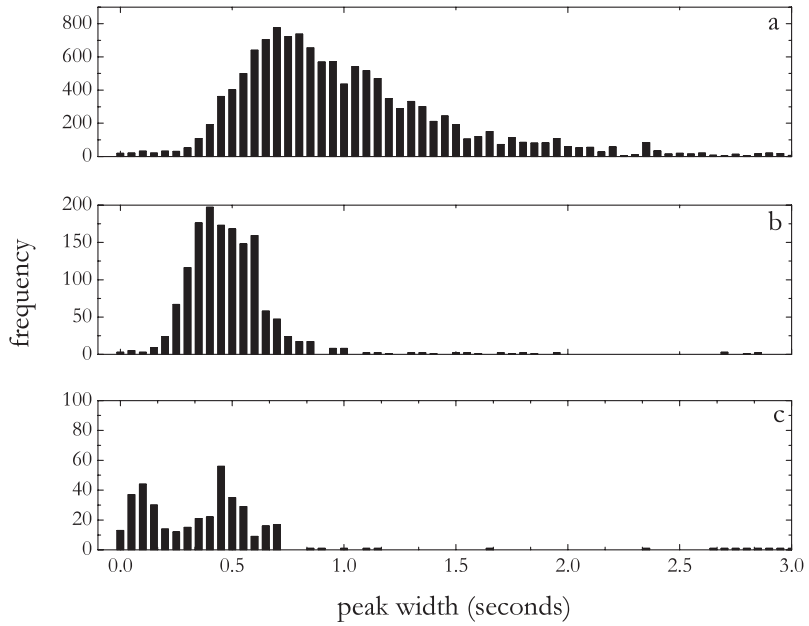

Figure 5. Burst width distributions extracted from bubble burst scans: (a) immediately after opening, (b) after 24 h and (c) when the drink has been completely degassed.

1.067, 0.599 and 0.386 s respectively. It can be seen that in addition to a reduction in average burst width with time, the distribution width also increases. This can be seen from the relative standard deviations (RSDs) of the distributions (24, 48 and 51% for 5, 12 and 24 h after opening respectively). Another interesting observation is that the histogram maxima decrease sharply with time over a 24 h period. This shows that although the average bubble size decreases over time, the range of bubble sizes increases over time. This suggests that not only does the rate of nucleation and growth of bubbles in the sample slow, but that some secondary mechanism of growth manifests. It is possible that the bimodal distribution observed in figure 5(c) is due to the aspiration of externally formed bubbles from the reservoir. After 24 h the bubbles in sample A remain small enough not to be excluded by the sampling capillary.

A clearer trend in the change in bubble size was demonstrated by the analysis of champagne samples. The de-gas process of champagne was monitored over a period of 24 h and data were extracted at intervals of 2 min for the first hour and 1 h for the next 24 h. The average interburst time, mean burst width and autocorrelation were calculated for each dataset (figure 6). Figure 6(a) reveals an increase in the average inter burst time from 1.5 to 20 s, which in turn demonstrates a decreasing rate of bubble formation with time. This decrease in rate is due to the reduction in carbon dioxide concentration. The decrease in bubble size could be further demonstrated by an autocorrelation analysis (figure 6(b)).

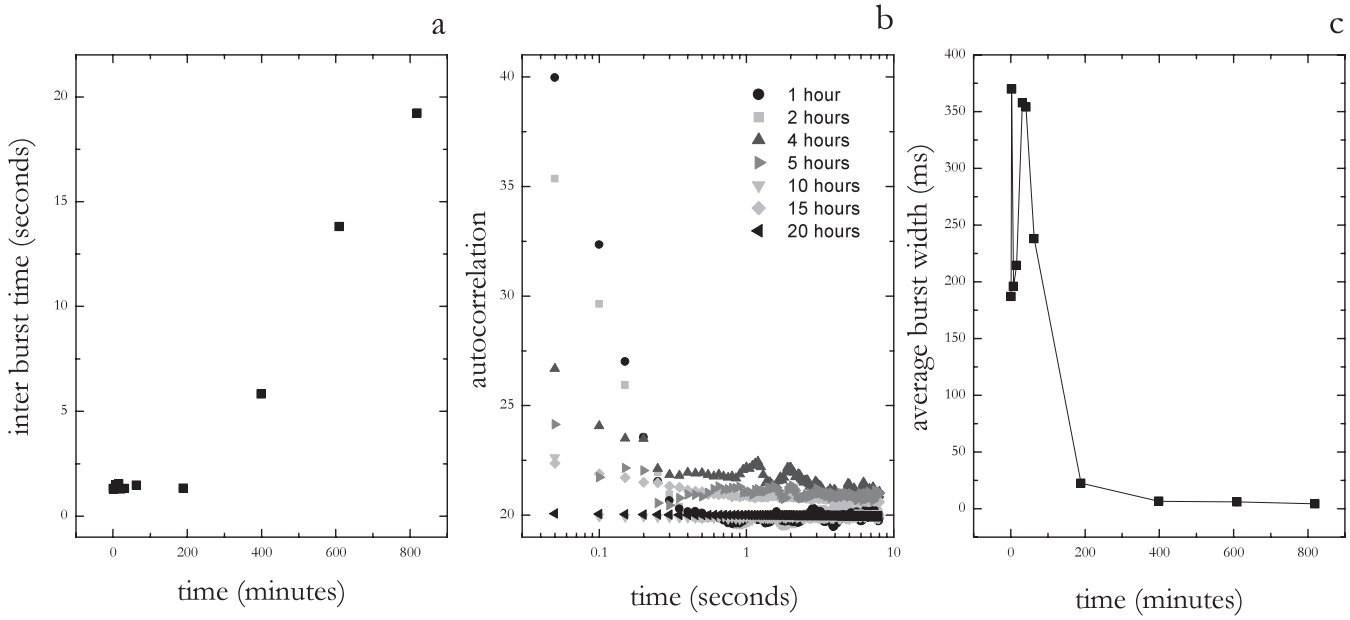

Figure 6. (a) Variation of average interburst time as a function of time after opening for champagne. Data are obtained every 2 min during the first hour and every hour over the next 24 h. (b) Autocorrelation analysis of champagne at various times after opening. (c) Average burst width recovered from champagne samples as a function of time. Data are obtained every 2 min during the first hour and every hour for the next 24 h.

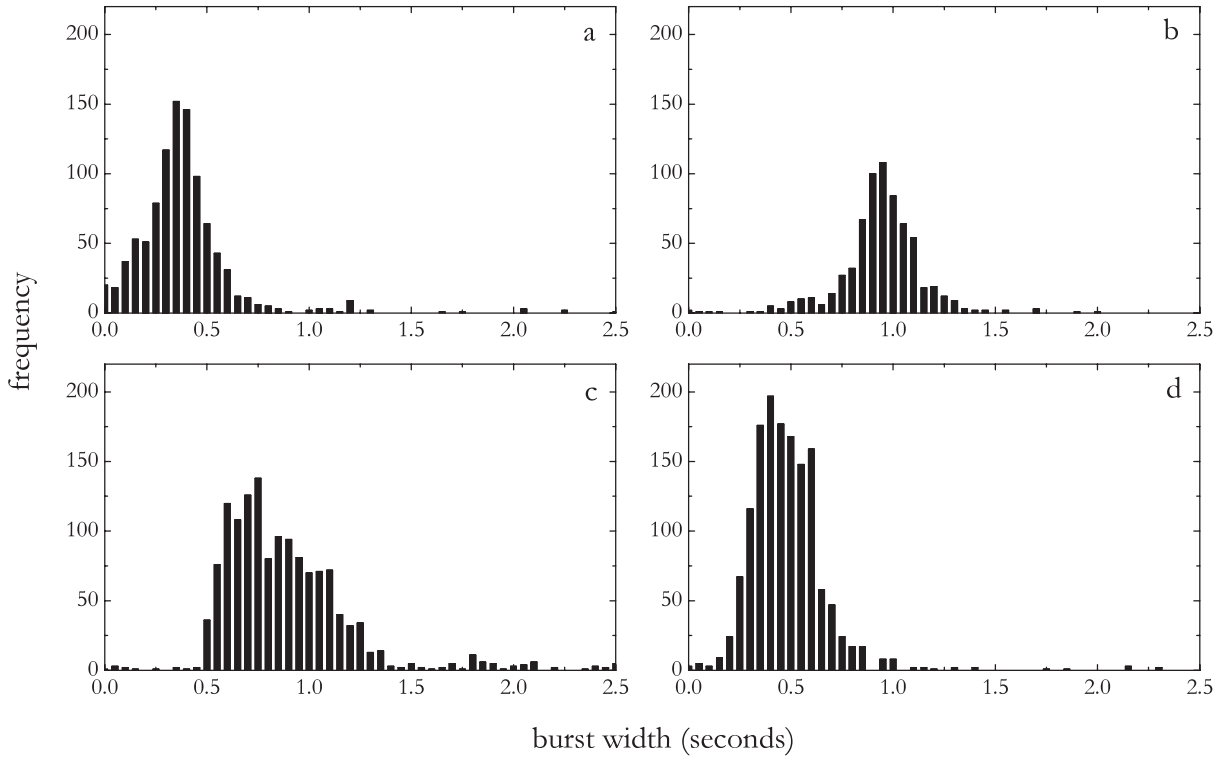

Figure 7. Burst width distributions extracted from bubble burst scans from samples A–D over a period of 18 h.

Such an analysis is useful in this instance as it gives valuable information pertaining to bubble residence times as well as intensities within the detection probe volume. It also provides qualitative information regarding changes in burst widths and areas when comparing several spectra. The autocorrelation curves in figure 6(b) were calculated using bubble burst scans for champagne measured at 1, 2, 4, 5, 10, 15, 20 h after opening the bottle. In all cases the autocorrelation curves were normalized over the total number of peaks. The autocorrelation curve generated immediately after opening yields a maximum value of 40.9 (sum squared of all counts). After an hour this value decreases to 35.9 and then to a minimum value of 19.5 after 20 h. This trend demonstrates that bubbles decrease in both size and frequency as a function of time. The average burst width shows a slightly more interesting trend (figure 6(c)). At early times the mean burst width is approximately 1.65 s. It then increases and reaches a maximum at 3.44 s before subsequently decreasing. This can be explained by

the thermodynamic process of carbon dioxide effervescence. Upon removing the cork from the champagne bottle, there is an abrupt change in pressure. To regain thermodynamic stability (corresponding to atmospheric pressure), carbon dioxide gas tries to escape from the supersaturated solution, thus forming bubbles. The rate of bubble growth initially increases with time and then decreases gradually (a limiting size is illustrated by the maximum in the curve). This can be explained in terms of the simple post nucleation growth being dependent upon the overall CO_2 concentration in the champagne: as time goes on the concentration reduces and the size of bubbles formed in the solution decreases to a burst width of 0.05 s. Another interesting observation was the increase in the RSD of the average burst width with time from 16 to 75%, illustrating that the smaller the size of the gas bubble, the greater the relative variation in size.

An investigation of the size of gas bubbles formed by four different carbonated beverages (samples A–D) was performed over a period of 18 h. Burst width distributions are shown in figure 7. It can be seen that all four beverages have different width distributions with respect to both mean bubble size (0.41, 0.75, 0.94 and 0.32 s) and distribution variance. Since the burst width is proportional to the bubble size, sample D is found to have the smallest bubbles formed while sample C has the largest. Bubbles sensed within the system fall between the limits of 50 and 400 μm. The lower limit can be improved by employing smaller channels, although this would tend to increase the head drop across the system. The upper limit can also be varied slightly but is dependent upon complex flow characteristics within the channel network. Larger bubbles tend to break down the slug/bubbly flow regime into a metastable, co-laminar flow regime, leading to results that are more difficult to interpret.

7. Conclusions

In conclusion we have reported a simple method for high-throughput analysis of gas bubbles in gas/liquid binary systems. The combination of a planar microfluidic device (for bubble manipulation) and refractive index detection (for bubble analysis) affords the detection and analysis of bubbles between 50 and 400 μm in diameter. The approach has been shown to be efficient due to the large differences in refractive indices of gases and liquids and the ability to rapidly motivate samples though microchannels. Statistical analysis of bubble burst scans (in terms of autocorrelation curves, burst width distributions and interburst time curves) yields information relating to both the size of bubbles and the frequency of bubble formation. Current studies are focusing of the use of maximum likelihood estimator methods to extract precise size information from single bursts within bubble burst scans [11]. In addition, these methods are also being further developed to provide for on-line reaction monitoring in microfluidic environments.

Acknowledgments

JBE acknowledges the receipt of an Overseas Research Studentship from the UK Government and SL is grateful to AstraZeneca for provision of an industrial research studentship.

References

[1] Zollinger H 1994 *Diazo Chemistry* vol 1 (Weinheim: VCH)
[2] Lin S M, Waterman D R and Lettington A H 2000 Measurement of droplet velocity, size and refractive index using the pulse displacement technique *Meas. Sci. Technol.* **11** L1–4
[3] Barigou M and Greaves M 1991 A capillary suction probe for bubble size measurement *Meas. Sci. Technol.* **2** 318–26
[4] Kawaguchi T, Akasaka Y and Maeda M 2002 Size measurements of droplets and bubbles by advanced interferometric laser imaging technique *Meas. Sci. Technol.* **13** 308–16
[5] Jakeway S C, de Mello A J and Russell E L 2000 Miniaturised total analysis systems for biological analysis *Fresenius J. Anal. Chem.* **366** 525–39
[6] Reyes D R, Iossifidis D, Auroux P A and Manz A 2002 Micro total analysis systems. 1. Introduction, theory and technology *Anal. Chem.* **74** 2623–36
[7] Kopp M U, de Mello A J and Manz A 1998 Chemical amplification: continuous-flow PCR on a chip *Science* **280** 1046–8
[8] Shafer N E and Zare R N 1991 Through a beer glass darkly *Phys. Today* **44** 48–52
[9] Edel J B and de Mello A J 2003 Single particle confocal fluorescence spectroscopy in microchannels: dependence of burst width and burst area distributions on particle size and flow rate *Anal. Sci.* **19** 1065–9
[10] Burns J R and Ramshaw C 2001 The intensification of rapid reactions in multiphase systems using slug flow in capillaries *Lab. Chip.* **1** 10–5
[11] Edel J B and de Mello A J 2003 Determination of single particle flow velocities in microchannels using a maximum likelihood estimator method *Phys. Chem. Chem. Phys.* **5** 3973–8